INORGANIC CHEMISTRY FRONTIERS

RESEARCH ARTICLE

View Article Online
View Journal | View Issue

Cite this: *Inorg. Chem. Front.*, 2025, **12**, 2897

A potential UV nonlinear-optical crystal with a strong second-harmonic response: $RbNa_2Eu_2(BO_3)_3$†

Dan Li,[a] Jingyu Shang,[b] Ming Gao,[c] Jiangtao Fan,*[a,e] Zhanggui Hu,*[a,e] Ping Peng[d] and Yicheng Wu[a]

Received 27th December 2024,
Accepted 6th February 2025

DOI: 10.1039/d4qi03330b

rsc.li/frontiers-inorganic

Ultraviolet (UV) nonlinear optical (NLO) crystals with a second-harmonic generation (SHG) response can efficiently output UV coherent light, and have important applications in UV solid-state lasers. Herein, we designed and synthesized a novel Eu-based borate (NLO) crystal, $RbNa_2Eu_2(BO_3)_3$ (RNEBO), which introduces Eu into an $A_3RE_2(BO_3)_3$ (A = alkali metal, RE = rare earth) system applied in the UV region first and exhibits both strong SHG activity and a wide optical transmission window. The RNEBO crystallizes in the non-centrosymmetric (NCS) space group *Amm*2, featuring a three-dimensional framework of $[EuBO_3]_\infty$ layers with isolated $[BO_3]^{3-}$ groups bridging in a coplanar arrangement. Meanwhile, the alkali metals Rb and Na were incorporated into the void of the anion framework to ensure coordination and charge balance. The distinctive internal structure enables RNEBO to possess a large SHG response (~3.55 × KDP) and UV transmittance of 6.17% at 200 nm. This finding confirms that RNEBO is a potential UV NLO crystal and provides valuable insights for the exploration of Eu-based borate UV NLO crystals in the future.

1. Introduction

Ultraviolet (UV)/deep ultraviolet (DUV) nonlinear optical (NLO) crystals as the core device medium for UV solid-state lasers with short wavelength outputting have great value of application in high power lasers, photoelectric communication, micromachining, microscopy, semiconductor lithography and other advanced frontier fields as they are capable of outputting coherent light by wave frequency conversion.[1–5] However, the development of UV/DUV NLO crystals remains limited, because it is restricted by the basic requirement of structure-oriented optical properties: (i) a short UV absorption cut-off edge (λ < 200 nm), (ii) a moderate birefringence for phase matching (Δn = 0.03–0.1@1064 nm), (iii) a non-centrosymmetric crystal structure to induce the second harmonic generation (SHG), and (iv) a large SHG efficiency, $d_{ij} > d_{36}$ KDP (0.39 p.m. per V) at 1064 nm. For decades, lots of crystals with excellent performance have been prepared, but only a few crystals can perfectly balance the above requirements due to the conflict between these requirements,[6] including $KBe_2BO_3F_2$(KBBF), which has a short UV cut-off edge (147 nm) and a large birefringence (Δn = 0.077@1064 nm). However, it is not particularly excellent due to the weak interlayer forces and the toxic raw material Be, which are not conducive to crystal growth.[5,7] Therefore, the exploration of UV/DUV nonlinear optical crystals with excellent properties is still urgent.

NLO crystals with a large SHG response are favored in the preparation of ultraviolet solid-state lasers because of their ability to output ultraviolet coherent light.[8–10] However, the reported NLO crystals with large SHG responses are still limited. As we know, NLO response may occur when crystals crystallize in non-centrosymmetric (NCS) space groups;[11] therefore, targeted construction of NCS NLO crystals is a prerequisite for large SHG intensity. Currently, the anionic groups usually include borate, carbonate, iodate, phosphate, *etc.*, such as $Sr_3BeB_6O_{13}$,[12] $Na_8Lu_2(CO_3)_6F_2$,[13] and $AZn(PO_3)_3$ (A = K, Rb).[14] Among them, borates are frequently selected as the ideal candidates due to their composition of π-conjugated or non-π-conjugated boronic anion groups and great tunable photoelectric properties. According to the anionic group theory, the $[BO_3]^{3-}$ group is the comparatively favorable building block in borates due to the

[a]*Tianjin Key Laboratory of Functional Crystal Materials, Institute of Functional Crystal, College of Material Science and Engineering, Tianjin University of Technology, Tianjin 300384, China. E-mail: fjt7023@163.com, hu@hfut.edu.cn*
[b]*School of Physics, Harbin Institute of Technology, Harbin 150001, China*
[c]*School of Computational Science and Electronics, Hunan Institute of Engineering, Xiangtan 411104, China*
[d]*School of Materials Science and Engineering, Hunan University, Changsha 410082, China*
[e]*College of Material Sciene and Engineering, Hefei University of Technology, Hefei, 230009, China*

†Electronic supplementary information (ESI) available. CCDC 2413055. For ESI and crystallographic data in CIF or other electronic format see DOI: https://doi.org/10.1039/d4qi03330b

π-conjugated electronic structure, and when the $[BO_3]^{3-}$ groups arrange in a coplanar manner with a large microscopic polarizability,[15] it is beneficial for achieving a wide transmission window in the UV region and large SHG response. Meanwhile, rare earth elements are also a hot spot in the selection of cations because of their large ionic radius and rich coordination environment. Highly distorted RE polyhedra contribute to the generation of the large SHG response, such as the reported rare earth-based borates $Cd_4SmO(BO_3)_3$ (1.2 × KDP),[16] $Cd_4TbO(BO_3)_3$ (1.5 × KDP),[16] $PrSc_3(BO_3)_4$ (1.85 × KDP),[17] *etc*. In addition, alkali metals with a large atomic radius, such as Rb and Cs, which can better fit to the anion framework, are also considered as suitable cations of NLO crystals, since they are capable of having large polarizability.[18] In addition, it has been reported that reducing the gap in the anion framework is beneficial for alleviating the phase transition.[6]

In this work, we successfully designed and synthesized a novel Eu-based borate NLO crystal, $RbNa_2Eu_2(BO_3)_3$ (RNEBO), which crystallized in the asymmetric space group *Amm*2. It is the first time that Eu is introduced into the $A_3RE_2(BO_3)_3$ (A = alkali metal, RE = rare earth) system applied in the UV region. It forms highly distorted $[EuO_9]$ polyhedra by sharing oxygen atoms with $[BO_3]^{3-}$, which further connect to the $[BO_3]^{3-}$ groups arranged in a coplanar manner forming the $[EuBO_3]_\infty$ layers as the anion framework of RNEBO, and Rb with a large atomic radius is introduced to fill the pores of the framework and increase polarizability. Considering that elements of the same main group have similar electronic structures and may exhibit chemical valence equivalent substitution, the light alkali metal Na is also introduced to balance the charge. Physicochemical characterization shows that RNEBO has transmission in the DUV region (200 nm, 6.17%) and exhibits a large SHG response (~3.55 × KDP), which prove that RNEBO is a promising UV NLO crystal.

2. Results and discussion

RNEBO crystallizes in the acentric orthorhombic space group *Amm*2 with the lattice parameters a = 5.1228(2) Å, b = 11.1226 (7) Å, c = 7.0441(4) Å and Z = 2. It is formed by three-dimensional $[EuBO_3]_\infty$ chains with $[BO_3]^{3-}$ groups bridged in a coplanar manner between infinite chains by sharing O atoms (Fig. 1d). In addition, alkali metal Rb and Na atoms are introduced into the gap of the three-dimensional frame to balance the charges of the coordinating O atoms. The asymmetric unit of RNEBO consists of one isolated Rb, two isolated Na, one isolated Eu, two isolated B, and four isolated O atoms, respectively, and Energy-Dispersive Spectroscopy (EDS) has been carried out to identify the elements contained (Fig. S1†). For B atoms, they bond with three O atoms to form a $[BO_3]^{3-}$ triangle structure with the B–O lengths lying within the range of 1.34 (2) Å to 1.40(4) Å. For Eu atoms, they are coordinated by nine O atoms to form a $[EuO_9]$ polyhedron with Eu–O distances of 2.381(2)–2.655(5) Å (Fig. 1b), which matches the reported results.[19] It is worth noting that the $[B(1)O_3]^{3-}$ triangle is arranged in a coplanar manner in the *bc* plane (Fig. 1a), which facilitates the generation of a large SHG response. Although

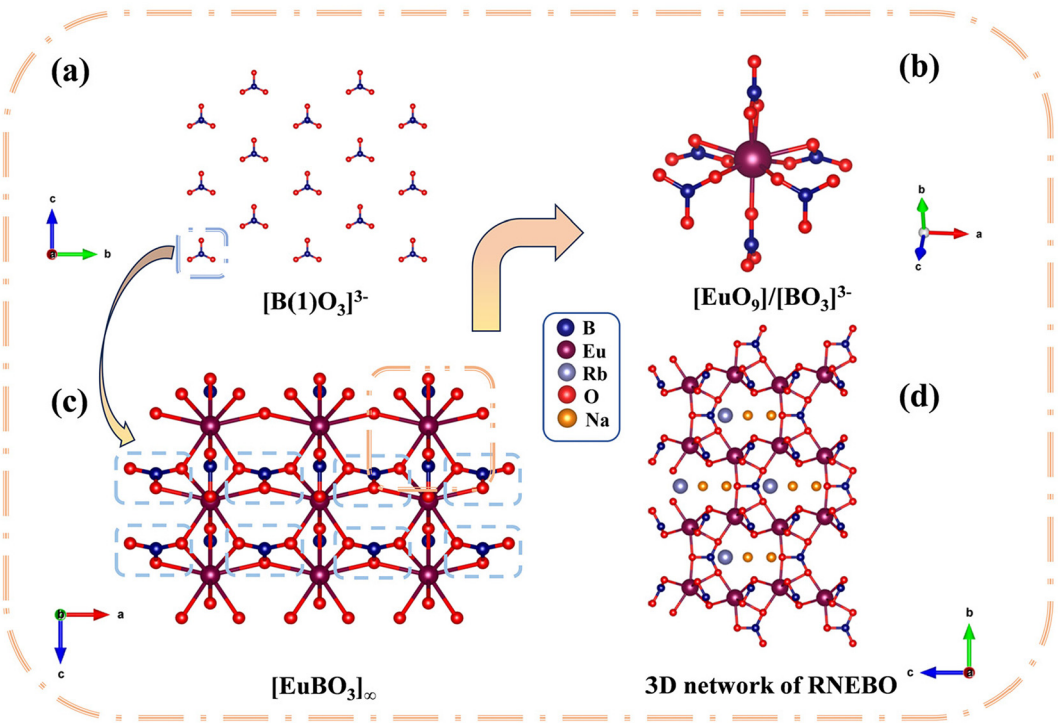

Fig. 1 (a) Coplanar arrangement of $[B(1)O_3]^{3-}$ units between the $[EuBO_3]_\infty$ layers. (b) Coordination of the $[EuO_9]$ polyhedron with $[BO_3]^{3-}$ units. (c) $[EuBO_3]_\infty$ chains with $[BO_3]^{3-}$ groups bridged between infinite chains along the *b* axis. (d) 3D network of RNEBO viewed along the *a* axis.

the $[B(2)O_3]^{3-}$ groups are not the coplanar and parallel arrangement, which has possible to counteract part of the microscopic polarizability. However, the increase in the density of $[BO_3]^{3-}$ groups can promote the production of a large SHG effect to some extent. At the same time, the introduced alkali metal Na and Rb atoms fill the frame holes and eliminate the end oxygen of $[BO_3]^{3-}$ groups as much as possible, which is conducive to the blue-shift of the UV cut-off edge. In addition, the $[BO_3]^{3-}$ groups bridged between $[EuBO_3]_\infty$ layers have greater connectivity than the F–K bond in KBBF, which is beneficial for improving the traditional layered growth during crystal growth and facilitating the growth of large crystals (Fig. 1c).

The phase purity of RNEBO was confirmed by powder X-ray diffraction (PXRD), which shows a good agreement with the theoretical crystal phase and indicates that we have successfully prepared the pure polycrystalline powder phase of RNEBO (Fig. 2a). The existence and behavior of the B–O groups of RNEBO are confirmed by Fourier transform infrared spectroscopy (Fig. 2c) – the vibration peak at 1209 cm^{-1} is mainly caused by the asymmetric stretching and symmetric vibration of $[BO_3]^{3-}$ groups, and the vibration peaks at 734 cm^{-1} and 595 cm^{-1} can be attributed to the unique bending vibration generated between B–O bonds.[20] In addition, the NLO property of RNEBO was also measured and is shown in Fig. 2d. The UV–vis–NIR reflectance spectra show that RNEBO has 6.17% UV transmission at 200 nm and possesses a wide optical band gap (4.08 eV), suggesting its potential application as a UV nonlinear optical crystal material. Several sharp peaks appearing at 361 nm, 381 nm, 396 nm, 415 nm, 465 nm, 533 nm and 587 nm are attributed to the $^7F_0 \rightarrow {}^5D_4$, $^7F_0 \rightarrow {}^5G_{2,3}$, $^7F_0 \rightarrow {}^5L_6$, $^7F_0 \rightarrow {}^5D_3$, $^7F_0 \rightarrow {}^5D_2$, $^7F_1 \rightarrow {}^5D_1$ and $^7F_1 \rightarrow {}^5D_0$ transitions of Eu^{3+}, respectively[21] (Fig. S2†). Thermogravimetric (TG) and DSC analyses were performed to explore the melting behavior of RNEBO (Fig. 2b), which showed that there was no significant weight loss on the TG curve, but a small endothermic peak was observed at 1038 °C, which suggested that RNEBO melts congruently and indicated that RNEBO has great thermal stability.

Since RNEBO crystallizes in the non-centrosymmetric space group *Amm*2, it is expected to exhibit SHG activity. Therefore, powder SHG responses of RNEBO with different particle sizes were adopted with radiation at 1064 nm. As shown in Fig. 3a and b, the SHG response of RNEBO gradually increase as the particle sizes increasing with the same particle sizes range from 163 to 200 μm. It proves that RNEBO is phase-matchable. Additionally, RNEBO exhibits a strong SHG efficiency of 3.55 × KDP, which is 2.96 times that of KBBF[6] and larger than that of some recently reported rare-earth borates, such as $Na_3Gd_2(BO_3)_3$ (1.3 × KDP),[22] $Ba_7(BO_3)_3F_5$ (1/3 × KDP),[23] $K_3Y_3(BO_3)_4$ (2 × KDP),[24] β-$KBe_2B_3O_7$ (0.75 × KDP),[25] $Ca_5(BO_3)_3F$ (2 × KDP),[26] $Na_3Sm_2(BO_3)_3$ (1 × KDP),[27] $Tb_{1.09}Al_{2.91}(BO_3)_4$ (1.53 × KDP),[28] $Sr_5La(BO_3)_4Cl$ (2.3 × KDP),[29] and $Sr_5La(BO_3)_4Br$ (2.4 × KDP),[29] as shown in Fig. 4. RNEBO exhibits excellent performance in the borate oxide system. According to the anionic group theory proposed by Academician Chen, when $[BO_3]^{3-}$ groups are arranged in a coplanar manner, it will be conducive to the generation of a large SHG

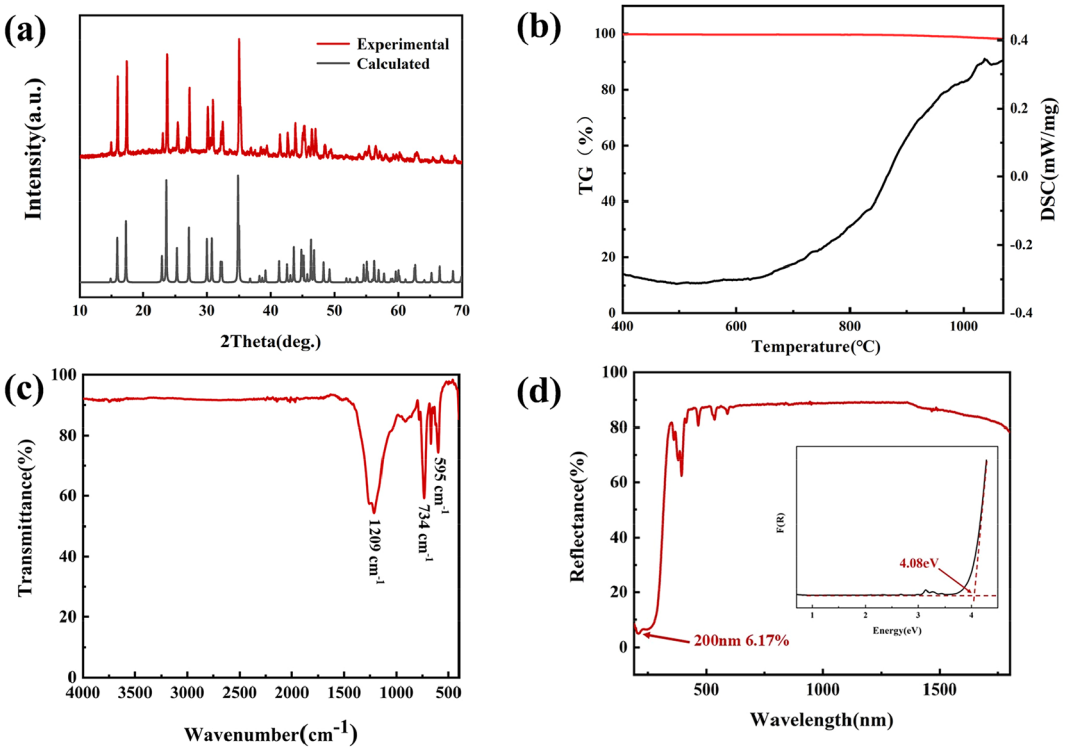

Fig. 2 PXRD patterns (a) and the infrared spectrum (c) of RNEBO. (b) TG and differential scanning calorimetry (DSC) curves of RNEBO. (d) UV–vis–NIR diffuse reflectance spectrum.

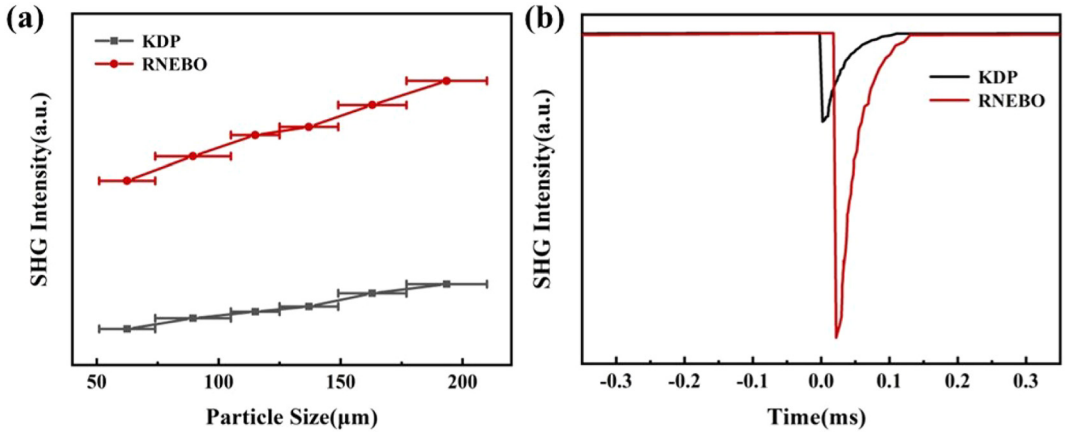

Fig. 3 Powder SHG measurements of RNEBO with KDP as a reference at 1064 nm.

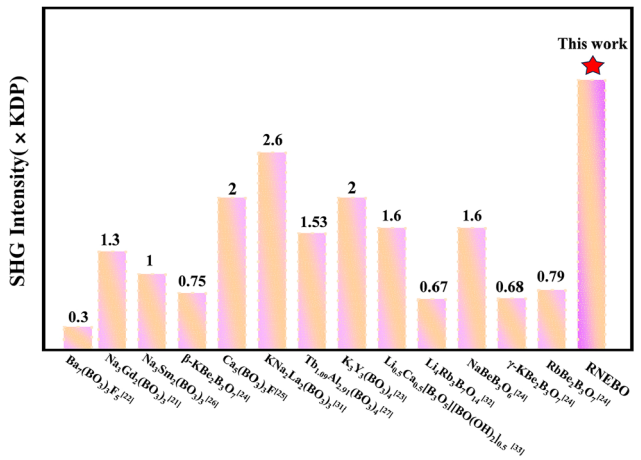

Fig. 4 Comparison of the SHG intensity with that of different crystals containing borates.[31]

response intensity.[30] In the RNEBO crystal structure, the $[B(1)O_3]^{3-}$ groups arrange in a beneficial coplanar manner in the *b c* plane, which is the main reason for the large SHG response. Although there is a dihedral angle among $[B(2)O_3]^{3-}$ groups, it does not completely counteract their microscopic second-order polarization. In addition, the distorted $[EuO_9]$ polyhedron possessing large microscopic polarizability also makes significant contribution to the large SHG response of RNEBO which cannot be ignored, comparable to that of $[LaO_9]$ in $KNa_2La_2(BO_3)_3$.[31] In summary, the synergistic interaction between the partially coplanar $[BO_3]^{3-}$ groups and the highly distorted $[EuO_9]$ polyhedra results in the outstanding SHG response of RNEBO.

Moreover, in order to further explore the optical properties in the microscopic mechanism of RNEBO, we employed first-principles calculations on the electronic structure and optical properties by the plane-wave pseudopotential method implemented in the CASTEP package based on DFT (density functional

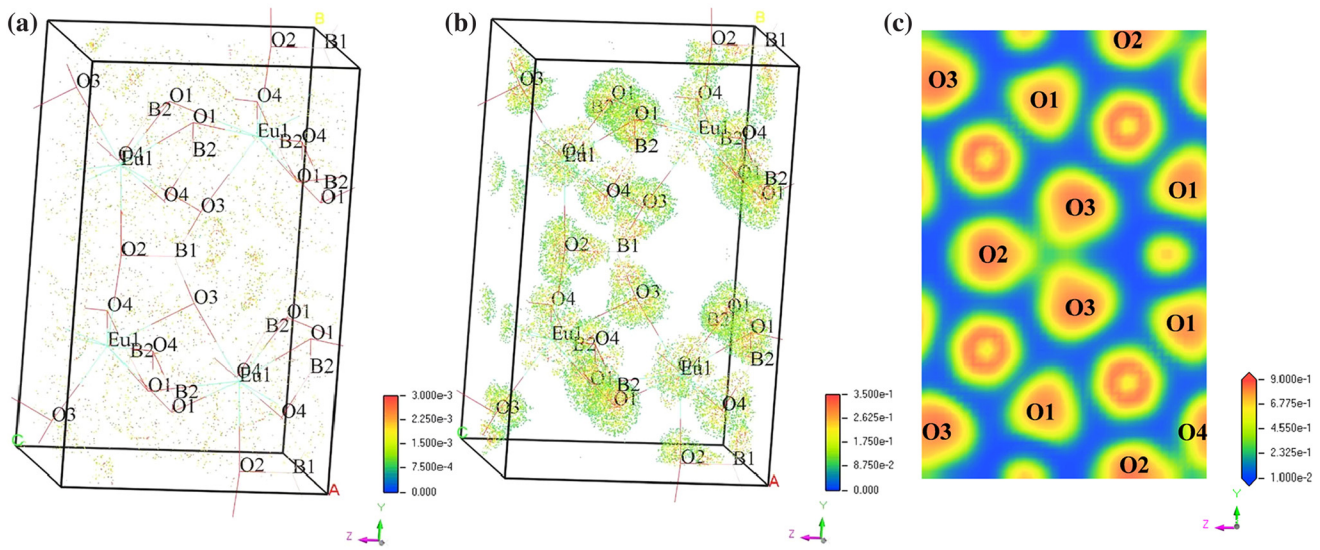

Fig. 5 The unoccupied (a) and occupied (b) SHG densities of RNEBO. (c) The electron localization function (ELF) map of RNEBO.

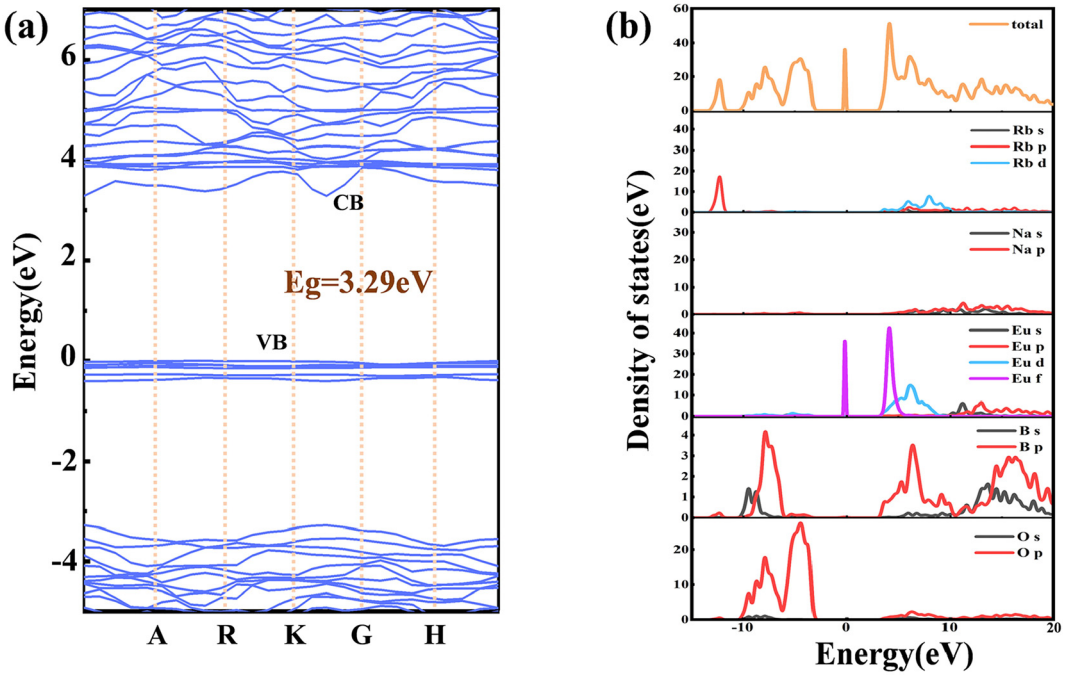

Fig. 6 (a) The electronic band structure calculated for RNEBO. (b) DOS and partial DOS projected for RNEBO.

theory).[32–36] RNEBO has a moderate birefringence (0.02 at 1064 nm), as shown in Fig. S3.†

To visualize the orbitals that contribute to the SHG effects of RNEBO, the SHG density maps of unoccupied and occupied states were obtained and are shown in Fig. 5a and b. For unoccupied states, the SHG densities of O atoms play a dominant role. For occupied states, the B and O atoms accumulate mainly, proving the significant contribution of $[BO_3]^{3-}$ groups. Meanwhile, the O atoms in $[EuO_9]$ polyhedra exhibit large SHG densities, which indicates that the $[EuO_9]$ polyhedra may also play important roles in the SHG process. Therefore, the contribution of the highly distorted $[EuO_9]$ polyhedra is also significant. Additionally, as shown in Fig. 5c, the ELF of RNEBO similarly exhibits the SHG activity of $[BO_3]^{3-}$ groups, confirming that the $[BO_3]^{3-}$ triangle plays a major role in SHG response. As shown in Fig. 6a, the DFT calculated results reveal that the band gap of RNEBO is 3.29 eV, which is mildly smaller than the experimental values resulting from the discontinuity of the exchange–correlation energy functional.[32] Clearly, the nonlinear optical properties mainly depend on the transition of electronic states near the Fermi level.[37,38] The density of states (DOS) and PDOS of RNEBO are plotted in Fig. 6b, and it can be observed that the top of the valence band (VB) from −7 to 0 eV is mainly dominated by O 2p, B 2p and Eu 4f orbitals, indicating the strong interaction between B–O and Eu–O bonds.[23] However, the bottom of the conduction bands (CBs) consists of B 2p, Eu 4f and partial Eu 4d orbitals. Therefore, the optical performances of RNEBO are mainly contributed by $[BO_3]^{3-}$ groups and the highly distorted $[EuO_9]$ polyhedra, which is consistent with the results of the above analysis.

3. Conclusions

In summary, we have successfully introduced Eu into an $A_3RE_2(BO_3)_3$ (A = alkali metal, RE = rare earth) system applied in the UV region for the first time and synthesized a new NLO UV crystal, $RbNa_2Eu_2(BO_3)_3$ (RNEBO), which crystallized in the asymmetric space group *Amm*2. RNEBO has a partially coplanar arrangement of $[BO_3]^{3-}$ groups and highly distorted $[EuO_9]$ polyhedra, which bring about excellent NLO performance compared to other recently reported rare-earth borates. RNEBO has 6.17% UV transmission at 200 nm and exhibits a large SHG response (~3.55 × KDP), which show that RNEBO will be an excellent NLO crystal material suitable for the ultraviolet window and provides valuable insights for the exploration of Eu-based borate NLO crystals in the future.

Author contributions

Dan Li: experiment, data analysis and writing – original draft. Jingyu Shang: data integration. Ping Peng and Ming Gao: theoretical calculations. Jiangtao Fan, Zhanggui Hu and Yicheng Wu: supervision, review and editing, funding acquisition and resources.

Data availability

The data supporting this article have been included within the manuscript and the ESI.† Crystallographic data for [2413055]

have been deposited at the CCDC.† The article provides sufficient experimental evidence and data to ensure reproducibility of the work.

Conflicts of interest

There are no conflicts to declare.

Acknowledgements

This study was supported by the Program for the National Key R&D Program of China (Grant No. JZ2023ZDYF0679) and the Anhui Science and Technology Plan Program (Grant No. 2408085QA001).

References

1 B. Dalai and S. K. Dash, Deep-ultraviolet (DUV) nonlinear optical (NLO) crystals: An application in photonic technologies, *Opt. Mater.*, 2023, **143**, 113909.
2 D. Guichaoua, B. Kulyk, V. Smokal, A. Migalska-Zalas, O. Kharchenko, O. Krupka, O. Kolendo and B. Sahraoui, UV irradiation induce NLO modulation in photochromic styrylquinoline-based polymers: Computational and experimental studies, *Org. Electron.*, 2019, **66**, 175–182.
3 T. Shanmugavadivu and M. Dhandapani, Crystal structure, spectral, thermal, optical, laser damage, NLO study and quantum chemical calculations of a noncentrosymmetric crystal N, N′-diphenylguanidinium p-toluenesulphonate, *J. Mol. Struct.*, 2019, **1179**, 651–661.
4 J. Chen, P. Yang, H. Yu, Z. Hu, J. Wang, Y. Wu and H. Wu, Designing a Strong Second-Harmonic Generation Polar Iodate by the Structure-Directing Properties of the "Tumbler-like" $[Zn(IO_3)(I_2O_5(OH))]$ Polyanions, *ACS Mater. Lett.*, 2023, **5**, 1665–1671.
5 J. Wang, H. Wu, Z. Hu, J. Wang, Y. Wu and H. Yu, A promising ultraviolet nonlinear optical crystal: $Rb_3Ba_3Li_2Al_4B_6O_{20}F$—crystal growth, physical properties, and 266 nm laser generation, *J. Mater. Chem. C*, 2023, **11**, 1320–1328.
6 H. Liu, H. Wu, Z. Hu, J. Wang, Y. Wu and H. Yu, Cs(3)[(BOP)(2)(B(3)O(7))(3)]: A Deep-Ultraviolet Nonlinear Optical Crystal Designed by Optimizing Matching of Cation and Anion Groups, *J. Am. Chem. Soc.*, 2023, **145**, 12691–12700.
7 H. Yu, N. Z. Koocher, J. M. Rondinelli and P. S. Halasyamani, Pb(2) BO(3) I: A Borate Iodide with the Largest Second-Harmonic Generation (SHG) Response in the KBe(2) BO(3) F(2) (KBBF) Family of Nonlinear Optical (NLO) Materials, *Angew. Chem., Int. Ed.*, 2018, **57**, 6100–6103.
8 A. M. Hanninen, R. C. Prince and E. Potma, Triple Modal Coherent Nonlinear Imaging with Vibrational Contrast, *IEEE J. Sel. Top. Quantum Electron.*, 2019, **25**, 6800411.
9 L. Wang, Q. Sun and J. Li, Recent progress on sulfide infrared nonlinear optical materials with large SHG response and wide band gap, *Chin. J. Struct. Chem.*, 2023, **42**, 100013.
10 C. Xie, E. Tikhonov, D. Chu, M. Wu, I. Kruglov, S. Pan and Z. Yang, A prediction-driven database to enable rapid discovery of nonlinear optical materials, *Sci. China Mater.*, 2023, **66**, 4473–4479.
11 Y. Kuk, J. Kee and K. M. Ok, Chiral Ligand-Driven Systematic Synthesis of Coordination Polymers with Noncentrosymmetric Structures, *Chemistry*, 2022, **28**, e202200007.
12 W. Yao, H. Huang, J. Yao, T. Xu, X. Jiang, Z. Lin and C. Chen, $Sr_3BeB_6O_{13}$: a new borate in the $SrO/BeO/B_2O_3$ system with novel tri-six-membered ring $(BeB_6O_{15})_{10}$- building block, *Inorg. Chem.*, 2013, **52**, 6136–6141.
13 M. Luo, N. Ye, G. Zou, C. Lin and W. Cheng, $Na_8Lu_2(CO_3)_6F_2$ and $Na_3Lu(CO_3)_2F_2$: Rare Earth Fluoride Carbonates as Deep-UV Nonlinear Optical Materials, *Chem. Mater.*, 2013, **25**, 3147–3153.
14 T. Yu, L. Xiong, X. Liu, Y.-C. Yang, Z. Lin, L.-M. Wu and L. Chen, $AZn(PO_3)_3$ (A = K, Rb): Deep-Ultraviolet Nonlinear Optical Phosphates Derived from Synergy of a Unique $[ZnO_6]$ Octahedron and a $[PO_3]_\infty$ Chain, *Cryst. Growth Des.*, 2021, **21**, 2445–2452.
15 Y. Song, M. Luo, C. Lin and N. Ye, Structural Modulation of Nitrate Group with Cations to Affect SHG Responses in RE $(OH)_2NO_3$ (RE = La, Y, and Gd): New Polar Materials with Large NLO Effect after Adjusting pH Values of Reaction Systems, *Chem. Mater.*, 2017, **29**, 896–903.
16 M.-Y. Cao, C.-L. Hu, P.-F. Chen, Q. Wang, B.-X. Li, Y. Lin and J.-G. Mao, $Cd_4REO(BO_3)_3$ (RE = Sm, Eu, Tb): three new cadmium–rare earth oxyborates with both good NLO and luminescence properties, *CrystEngComm*, 2022, **24**, 2542–2550.
17 A. Y. Jamous, A. B. Kuznetsov, K. A. Kokh, V. A. Svetlichnyi, N. G. Kononova, V. S. Shevchenko, A. A. Ryadun and A. E. Kokh, Study of RBO_3-$ScBO_3$ phase diagrams and $RSc_3(BO_3)_4$ orthoborates (R = La, Pr and Nd), *J. Alloys Compd.*, 2022, **905**, 164162.
18 V. V. Atuchin, A. K. Subanakov, A. S. Aleksandrovsky, B. G. Bazarov, J. G. Bazarova, T. A. Gavrilova, A. S. Krylov, M. S. Molokeev, A. S. Oreshonkov and S. Y. Stefanovich, Structural and spectroscopic properties of new noncentrosymmetric self-activated borate $Rb_3EuB_6O_{12}$ with B_5O_{10} units, *Mater. Des.*, 2018, **140**, 488–494.
19 Y. Chi, H. G. Xue and S. P. Guo, Designing Sulfide Borate as a Novel Type of Second-Order Nonlinear-Optical Material, *Inorg. Chem.*, 2020, **59**, 1547–1555.
20 M. Yang, H. Yu, Z. Hu, J. Wang, Y. Wu and H. Wu, Ba(2) ScBSi(2)O(9): A Mixed-Coordination Borosilicate with a Low B/Si Ratio Exhibiting Enhanced Second Harmonic Generation Response, *Inorg. Chem.*, 2024, **63**, 16507–16514.
21 W. Zhou, R. Zhuang, W. Zhao, G. Wang, L. Zhang, J. Ma, X. Bao, F. Wang and Y. Chen, Second harmonic generation

in $Na_3Gd_2(BO_3)_3$ crystals, *Cryst. Res. Technol.*, 2011, **46**, 926–930.
22 M. L. Meena, C. H. Lu, S. Som, R. Chaurasiya and S. D. Lin, Highly efficient and thermally stable Eu^{3+} activated phosphate based phosphors for wLEDs: An experimental and DFT study, *J. Alloys Compd.*, 2022, **895**, 162670.
23 J. Liu, Synthesis, crystal structure and optical properties of a new nocentrosymmetric borate: $Ba_7(BO_3)_3F_5$, *Mater. Res. Bull.*, 2016, **81**, 114–118.
24 C. Feng, H. Wu, Z. Hu, J. Wang, Y. Wu and H. Yu, K(3)Y(3)(BO(3))(4): A Potential UV Nonlinear-Optical Crystal Designed by a Chemical Substitution Strategy, *Inorg. Chem.*, 2024, **63**, 17362–17366.
25 S. Wang, N. Ye, W. Li and D. Zhao, Alkaline Beryllium Borate NaBeB3O6 and ABe2B3O7 (A = K,Rb) as UV Nonlinear Optical Crystals, *J. Am. Chem. Soc.*, 2010, **132**, 8779–8786.
26 G. Chen, Y. Wu and P. Fu, Growth and characterization of a new nonlinear optical crystal $Ca_5(BO_3)_3F$, *J. Cryst. Growth*, 2006, **292**, 449–453.
27 G. Zhang, Y. Wu, P. Fu, G. Wang, H. Liu, G. Fan and C. Chen, A new sodium samarium borate $Na_3Sm_2(BO_3)_3$, *J. Phys. Chem. Solids*, 2002, **63**, 145–149.
28 A. B. Kuznetsov, A. Y. Jamous, M. I. Rakhmanova, E. A. Simonova, V. A. Svetlichnyi, A. E. Kokh, V. N. Yudin, S. F. Solodovnikov, V. S. Shevchenko and K. A. Kokh, Nonstoichiometry as a hidden aspect of TbAl(3)(BO(3))(4) optical properties, *Dalton Trans.*, 2024, **53**, 18653–18661.
29 B. Yuan, H. Wu, Z. Hu, J. Wang, Y. Wu and H. Yu, Deep Ultraviolet-Transparent Materials with Strong Second Harmonic Response, *Chem. Mater.*, 2022, **34**, 8004–8012.
30 Y. Shen, S. Zhao and J. Luo, The role of cations in second-order nonlinear optical materials based on π-conjugated $[BO_3]^{3-}$ groups, *Coord. Chem. Rev.*, 2018, **366**, 1–28.
31 J. Song, C. Li, J. Jiao, Y. She, W. Zhao, F. Liang, N. Ye, Z. Hu and Y. Wu, $KNa_2La_2(BO_3)_3$: a shortite-type lanthanide borate exhibiting strong nonlinear optical activity induced by isolated $[BO_3]$ triangles and distorted $[LaO_9]$ polyhedra, *Inorg. Chem. Front.*, 2023, **10**, 5488.
32 C.-A. Chen and G.-Y. Yang, Syntheses, structures and optical properties of two B_3O_7 cluster-based borates, *CrystEngComm*, 2022, **24**, 1203–1210.
33 R. Liu, H. Wu, H. Yu, Z. Hu, J. Wang and Y. Wu, $K_5Mg_2La_3(BO_3)_6$: An Efficient, Deep-Ultraviolet Nonlinear Optical Material, *Chem. Mater.*, 2021, **33**, 4240–4246.
34 F. Liang, C. He, D. Lu, Q. Fang, Y. Fu, H. Yu, H. Zhang and Y. Chen, Multiphonon-assisted lasing beyond the fluorescence spectrum, *Nat. Phys.*, 2022, **18**, 1312–1316.
35 Y. Cheng, F. Liang, D. Lu, J. Feng, G. Zhang, H. Yu, H. Zhang and Y. Wu, Phonon engineering in Yb: $La_2CaB_{10}O_{19}$ crystal for extended lasing beyond the fluorescence spectrum, *Light:Sci. Appl.*, 2023, **12**, 203.
36 P. Feng, J. Zhang, M. Ran, X. Wu, H. Lin and Q. Zhu, Rare-earth-based chalcogenides and their derivatives: an encouraging IR nonlinear optical material candidate, *Chem. Sci.*, 2024, **15**, 5869–5896.
37 Maria, J. Iqbal and K. Ayub, Enhanced electronic and nonlinear optical properties of alkali metal (Li, Na, K) doped boron nitride nano-cages, *J. Alloys Compd.*, 2016, **687**, 976–983.
38 B. Zhang, M. Ran, X. Wu, H. Lin and Q. Zhu, Recent advances and future perspectives on rare-earth-based nonlinear optical materials with π-conjugated [XO3] (X = B, C, N) units, *Coord. Chem. Rev.*, 2024, **517**, 216053.